

Full Length Article

Inherent selective pulsed chemical vapor deposition of aluminum oxide in nm scale

Yunil Cho^a, James Huang^b, Zichen Zhang^b, Kesong Wang^c, Ping-che Lee^b, Chanyoung Kim^d, Keith Wong^f, Srinivas Nemani^f, Ellie Yieh^f, Andrew C. Kummel^{e,*}^a Electrical and Computer Engineering Program, University of California, San Diego, La Jolla, CA 92093, United States^b Materials Science and Engineering Program, University of California, San Diego, La Jolla, CA 92093, United States^c Mechanical and Aerospace Engineering Program, University of California, San Diego, La Jolla, CA 92093, United States^d NanoEngineering Program, University of California, San Diego, La Jolla, CA 92093, United States^e Department of Chemistry & Biochemistry, University of California, San Diego, La Jolla, CA 92093, United States^f Applied Materials, Inc., Sunnyvale, CA 95054, United States

ARTICLE INFO

Keywords:

Inherent area selective deposition
 Aluminum oxide
 Water-free deposition
 Metal alkoxide precursor
 Nanoscale selective deposition

ABSTRACT

Inherent selective pulsed chemical vapor deposition (CVD) of aluminum oxide on Si and SiO₂ in preference to SiCOH has been studied. SiCOH is alkyl (-C_xH_y) terminated SiO₂, which was used as a non-reactive surface. For aluminum oxide deposition, pulsed CVD processes using aluminum tri *sec*-butoxide (ATSB) and trimethylaluminum (TMA) were tested. ATSB alone can induce a pulsed thermal CVD reaction to selectively deposit aluminum oxide at 300 °C sample temperature; ~4 nm of aluminum oxide were selectively deposited on Si and SiO₂ in preference to SiCOH. By adding a periodical pulse of TMA during ATSB pulses, higher selectivity was achieved with ~12 nm and ~14 nm of aluminum oxide on Si and SiO₂ with around 0.4–0.5 nm root mean square (RMS) roughness at 330 °C. The high selectivity persisted on the nanoscale: STEM showed that ~10 nm of aluminum oxide could be selectively deposited on nanoscale patterned features. The selectively deposited AlO_x films showed low k (~4) dielectric performance with low leakage (around 10⁻⁶ A/cm² at ± 2 V for a 15 nm thick film). This selective aluminum oxide pulsed CVD process has the potential to be applicable in nanoscale fabrication, such as low k spacer and etch stop layer.

1. Introduction

As nanoscale fabrication becomes an important issue in leading-edge semiconductor fabrication, area selective deposition of nanoscale features has become a field of interest. Area selective deposition of oxides can be applied to double patterning on the nanoscale [1,2]. In addition, selective oxide deposition can be employed for etch stop barriers [3,4] or dielectric-on-dielectric structures for fully self-aligned vias [5,6]. For selective deposition, three methods are available: inherent selective deposition, selective deposition using surface passivation, and selective deposition using activation. The inherent selective deposition uses reactivity differences between precursors and different surfaces [1,3,4,7–11]. This method is more desirable as it does not require additional steps for passivation or activation and, therefore, is often less sensitive to defects; however, few studies have been done about inherent selective deposition. The majority of selective depositions are based on

selective deposition using passivation. This method uses a passivant, such as long-chain alkanes, to prevent nucleation of precursors on a particular surface, thereby inducing selective deposition on an unpassivated surface [12–15]. In addition, selective activation, such as electron beam-induced ALD, can induce selective deposition [16–18]. However, selective activation requires additional steps to activate the surface and may require specific sample geometry.

CVD is a widely used deposition method in the semiconductor industry. Among various CVD methods, thermal CVD uses high sample temperature, which decomposes one or more precursors and forms reactive ligands such as hydroxyl (-OH) to promote film formation [1,3,4,8]. For selective oxide deposition, water-free deposition is desirable as water can induce poor selectivity [19] and damage metals and low k dielectrics, such as SiCOH. It was previously reported that metal alkoxide precursors could thermally decompose and form oxide films [1,3,4,8]. Since metal alkoxide precursors have abundant oxygen

* Corresponding author.

E-mail address: akummel@ucsd.edu (A.C. Kummel).<https://doi.org/10.1016/j.apsusc.2023.156824>

Received 25 December 2022; Received in revised form 9 February 2023; Accepted 18 February 2023

Available online 21 February 2023

0169-4332/© 2023 Elsevier B.V. All rights reserved.

on their ligands, no additional oxygen precursor, such as water, was required during deposition, which could improve the selectivity. For example, with the pulsed CVD process of titanium isopropoxide ($\text{Ti}(\text{O}^i\text{Pr})_4$) and hafnium tertbutoxide ($\text{Hf}(\text{O}^i\text{Bu})_4$), selective TiO_2 and HfO_2 deposition were achieved, respectively, on Si and SiO_2 in preference to SiCOH. SiCOH is porous methyl-terminated SiO_2 , a low k dielectric used in the semiconductor industry [20–23]. This selective deposition process with metal alkoxide precursors was also demonstrated with a passivation process which covers the sample surface with $-(\text{O})\text{C}_x\text{H}_y$ bonds [8]. However, as oxide films became thicker, crystallization occurred along with the resulting formation of a rough film. To solve the film roughness issue, selective oxide deposition with a nanolaminate structure was performed by periodically depositing two different oxide films [3,4]. However, the nanolaminate structure has the drawback of complicating the etching process for use as a temporary etch stop layer.

Al_2O_3 is a desirable material to selectively deposit because it is amorphous regardless of its thickness, reducing the risk of forming a rough surface. Al_2O_3 is also a well-known capping and dielectric layer in the semiconductor industry. L. Cao et al. studied AlO_x ALD using aluminum tri-sec-butoxide (ATSB) and oxygen precursors such as H_2O and O_2 plasma [24]. The authors showed that ATSB without coreactant has a thermal CVD reaction above 250 °C sample temperature. However, the study focused on the AlO_x ALD process using oxygen-containing coreactants and did not study selective deposition. Liu et al. [25] and Bobb-Semple et al. [12] studied selective AlO_x ALD. For AlO_x deposition, both studies used TMA and water, which is a commonly used AlO_x deposition method. For selective deposition, both Liu et al. and Bobb-Semple et al. used liquid phase octadecylphosphonic acid to passivate oxide or metal surfaces to have selective aluminum oxide deposition on the unpassivated surfaces. Liu et al. reported a maximum of ~30 nm of selective AlO_x deposition [25]. However, these studies focused on selective deposition using a passivant, not on inherent selective deposition nor selective deposition in the nm scale.

The present study investigated the inherent selective AlO_x CVD using ATSB and trimethylaluminum (TMA). The pulsed CVD with ATSB at 300 °C sample temperature demonstrated ~4 nm of selective AlO_x deposition on Si and SiO_2 in preference to SiCOH. TMA was employed since it has the potential to react with excess oxygen from nucleated metal alkoxide precursors to increase selectivity. Pulsed CVD with ATSB and TMA at 300 °C sample temperature increased the selectivity; ~10 nm of AlO_x were selectively deposited on Si and SiO_2 . However, excess TMA inhibited the film growth on Si and SiO_2 . Higher sample temperature (330 °C) increased the reactivity of ATSB; therefore, more TMA pulses could be added, inducing an increase in selectivity; 12 and 14 nm of AlO_x were selectively deposited on Si and SiO_2 . The AlO_x films were smooth with 0.4–0.5 nm RMS roughness. From the electrical characterization, the AlO_x film showed dielectric behavior with $k = \sim 4$ and around 10^{-6} A/cm² leakage current at ± 2 V; the desirable and unusual low dielectric constant of the AlO_x was consistent with substoichiometric composition. The pulsed CVD with ATSB and TMA at 330 °C sample temperature was tested on Cu/SiCOH nanoscale patterned sample and demonstrated ~10 nm of selective AlO_x deposition on the Cu surfaces and no detectable AlO_x on SiCOH.

2. Experimental

The inherent selective AlO_x pulsed CVD was tested on three different substrates with all Si-based with different surface bonds: Si (Si-H), SiO_2 (Si-OH), and SiCOH (Si- $(\text{O})\text{C}_x\text{H}_y$). The size of each substrate was $\sim 2 \times \sim 12$ mm. The samples were sequentially degreased with acetone, methanol, and deionized water for 15 s each. To remove surface native oxide, degreased Si and SiO_2 were wet cleaned in a 0.5% diluted hydrofluoric acid solution for 30 s. After the cleaning, the samples were blown with an N_2 air gun to remove residual solution on the sample surface. The three samples were loaded into the chamber on a single sample holder, so they had the same CVD process to quantify the

selectivity. For the nanoscale selectivity test, a Cu/SiCOH nanoscale patterned sample was used. The Cu/SiCOH sample was wet cleaned with the same degreasing process explained above. Since the SiCOH surface of the patterned sample was damaged from the initial chemical mechanical polishing (CMP) process, it was not fully covered with $-\text{OC}_x\text{H}_y$ or $-\text{C}_x\text{H}_y$ bonds. Therefore, to restore the damaged part, a silylation repair process was performed with 1,1,3,3-tetra-methyldisilazane (TMDS) [8,26]. The sample was soaked in TMDS gas with constant pressure of 10 Torr for 10 min at 70 °C sample temperature. After the passivation, the patterned sample was loaded with a blanket SiCOH sample to check selective deposition in the Cu region.

The vacuum chamber system consisted of three chamber parts (Fig. S1 shows a chamber schematic). A load lock chamber was employed to load and retrieve samples. It also worked as a buffer chamber between the deposition chamber and ultra-high vacuum (UHV) X-ray photoelectron spectroscopy (XPS) chamber to prevent gas phase precursor flows into the UHV chamber. The load lock chamber was pumped by a turbopump (Pfeiffer TPU 060) and a mechanical backing pump (Edwards RV3). The deposition chamber was also pumped by a turbopump (Pfeiffer TPU 060) and a mechanical backing pump (Edwards RV3). A Cu sample holder with a cartridge heater inserted inside was located at the end of the transfer arm of the deposition chamber. Dosing lines for ATSB, TMA, and N_2 purge gas were connected to the deposition chamber. The UHV chamber was employed for *in-vacuo* XPS. The chamber was pumped by an ion pump (Agilent Varian VacIon 300 StarCell) to UHV pressure (low 10^{-9} torr). The samples were transferred *in-vacuo* for XPS analysis to prevent exposure to the ambient air.

During the CVD process, the deposition chamber wall and dosing lines were kept at 150 °C. Samples were heated up to 300 °C and 330 °C using the cartridge heater inside the Cu platform. For the oxide deposition, pulsed CVD, instead of continuous dosing, was used to achieve good selectivity and to protect the turbopump. By calibrating the pneumatic valve open time and the precursor bottle temperature, a low mTorr range of precursor pulse pressure was maintained to have a selective deposition. Excessive precursor vapor pressure can induce unwanted CVD reactions, which can induce loss of selectivity or high film roughness and damage the turbopump. Lower pulse pressure is less preferable as it greatly increases the process time to grow a film of a given thickness. The ATSB bottle was heated to 110 °C to have sufficient vapor pressure. The TMA bottle was kept at room temperature (~ 21 °C). In addition, no push gas was used for both ATSB and TMA doses. The dosing line between the deposition chamber and the precursor bottles was kept at 150 °C to avoid precursor clogging inside the dosing line. The valve open time for each precursor was set to 800 ms and 15 ms for ATSB and TMA, respectively. The precursor pulses were monitored by the pressure spikes inside the chamber. A mass flow controller was not used in the dosing line in this study, which could induce instability in the growth rate for the CVD process. N_2 gas was continuously purged during the CVD process to remove the residual precursors inside the dosing chamber. AlO_x CVD was tested with the single precursor pulsed CVD with ATSB and the pulsed CVD with supercycle of ATSB and TMA. For ATSB single precursor pulsed CVD, three different purging times between each ATSB pulse were tested: 10, 60, and 240 s. For the supercycle with ATSB and TMA, one pulse of TMA was employed with every 80/120/160 ATSB pulses to check the effect of TMA pulse frequency on the selectivity of the CVD process. The purge time between different precursor pulses was set to 60 s. The purge time between ATSB pulses was set to 10 s. Both CVD processes were tested at 300 °C and 330 °C sample temperatures to check the effect of the sample temperature on the selectivity.

After the AlO_x deposition, *in-vacuo* XPS analysis was performed. A monochromatic Al K α source (1486.7 eV) and XM 1000 MkII/SPHERA (Omicron Nanotechnology) hemispherical analyzer were used for the measurement. The anode voltage, the filament emission current, and hemisphere analyzer pass energy were set to 10 kV, 25 mA, and 50 eV, respectively. The XPS detector was aligned to 30° from the sample

surface. The XPS analysis was performed with CASA XPS v.2.3 and utilized Shirley background subtraction. Each element composition was derived by normalizing to the sum of all elements. The oxide film thickness was derived from Si substrate signal attenuation from the XPS result [1,8]. When the Si signal was not detected (film thickness more than 4 nm), the thickness was measured by ex-situ ellipsometry (J. A. Woollam M-2000D). After the whole in-vacuo CVD and XPS, the ex-situ atomic force microscopy (AFM) (Park Systems XE7/tapping mode) and scanning transmission electron microscopy (STEM) (FEI F200X G2) were performed.

For the electrical characterization of the AlO_x film, capacitors were fabricated. The bottom electrode was the Si substrate, while thermal evaporation (Denton 502A) was employed to fabricate the top electrode (Ni). The Ni top electrode had a contact diameter of 150 μm and a thickness of 30 nm. For the post-deposition anneal, O_2 anneal (450 $^\circ\text{C}$ for 30 min), and sequential forming gas anneal (330 $^\circ\text{C}$, 350 $^\circ\text{C}$, and 380 $^\circ\text{C}$ three steps anneal for 15 min each) were employed. The capacitance–voltage (C-V) and current–voltage (I-V) characteristics of the capacitor were probed by the Keithley 4200A SCS parameter analyzer.

3. Results and discussion

3.1. Selectivity of the AlO_x pulsed CVD with aluminum tri-sec butoxide

The inherent selectivity of single precursor (ATSB) pulsed CVD was first tested. To check the reactivity difference between ATSB precursor and different surface bonds, Si, SiO_2 , and SiCOH , which are all Si-based but have different surface bonds, were used as a test sample set. ATSB pulses were dosed with constant purge time. Three purge times (10, 60, and 240 s) were tested to check if ATSB has reversible molecular adsorption on the SiCOH surface [8]. Fig. 1 shows the XPS chemical composition of Si, SiO_2 , and SiCOH surface during the ATSB pulsed CVD process at 300 $^\circ\text{C}$ sample temperature. Since L. Cao et al. showed that the thermal CVD reaction of ATSB started over 250 $^\circ\text{C}$ and fully dominated the deposition at ≥ 300 $^\circ\text{C}$ [24], the 300 $^\circ\text{C}$ sample temperature was first tested. The purge time between ATSB pulses was set to 10 s. (X-ray photoelectron spectra of each element-specific binding region are shown in Supporting Information Fig. S2.) At 300 $^\circ\text{C}$ sample temperature,

thermal decomposition of ATSB prevailed and induced AlO_x film deposition [24]. As more ATSB pulses were dosed, AlO_x films were formed on Si and SiO_2 surfaces, as shown in Fig. 1; Si signal composition became smaller, and Al signal appeared as the deposition continued. After 640 ATSB pulses, Si peaks were fully attenuated from Si and SiO_2 . The AlO_x thickness on Si and SiO_2 was 4.0 nm and 4.5 nm, respectively. On SiCOH , however, less than a monolayer (~ 0.2 nm) of AlO_x was deposited after 640 ATSB pulses. The selective deposition was due to the inherent reactivity difference of precursor-mediated chemisorption of ATSB.

ATSB pulsed CVD at 300 $^\circ\text{C}$ sample temperature was also tested with 60, and 240 s purge times. (The XPS analysis of ATSB pulsed CVD with 60 s and 240 s purge times are shown in Supporting Information Figs. S3 and S4, respectively.) However, no further increase in selectivity was detected. The CVD with 60 s purge time showed similar selectivity to the result with 10 s purge time. Selectivity became lower as the purge time was increased to 240 s. In sum, the ATSB pulsed CVD at 300 $^\circ\text{C}$ had a most selective process with a purge time between 10 and 60 s. As shown in Supporting information Fig. S5, the purge time also affects the growth rate; this was not expected. While the 60 and 240 s purges had similar growth rates, the 10 s purge had lower growth rate. This is consistent with a slow desorption from the surface; therefore, a longer purge allows more time for the molecules to react on the substrate. The 240 s purge had slightly lower growth rate than the 60 s purge; it is possible that this is because the very long purge reduces passivation of the chamber walls thereby causing more of each precursor pulse to stick to the chamber walls.

ATSB pulsed CVD was also tested at 330 $^\circ\text{C}$ sample temperature to check whether a higher sample temperature can improve selectivity. After 350 ATSB pulses, Si and SiO_2 had around 4.4 and 5.6 nm of AlO_x deposition, respectively (the XPS analysis is shown in Supporting Information Fig. S6). It was observed that the growth rate per ATSB pulse increased as the sample temperature increased. This higher temperature and consequently higher growth rate were used in the pulsed CVD process with ATSB and TMA in a later section. However, the CVD process at 330 $^\circ\text{C}$ showed similar selectivity compared to the result at 300 $^\circ\text{C}$ (around 4–5 nm of AlO_x on Si and SiO_2 and less than a monolayer (0.2–0.3 nm) of AlO_x on SiCOH), consistent with a large temperature

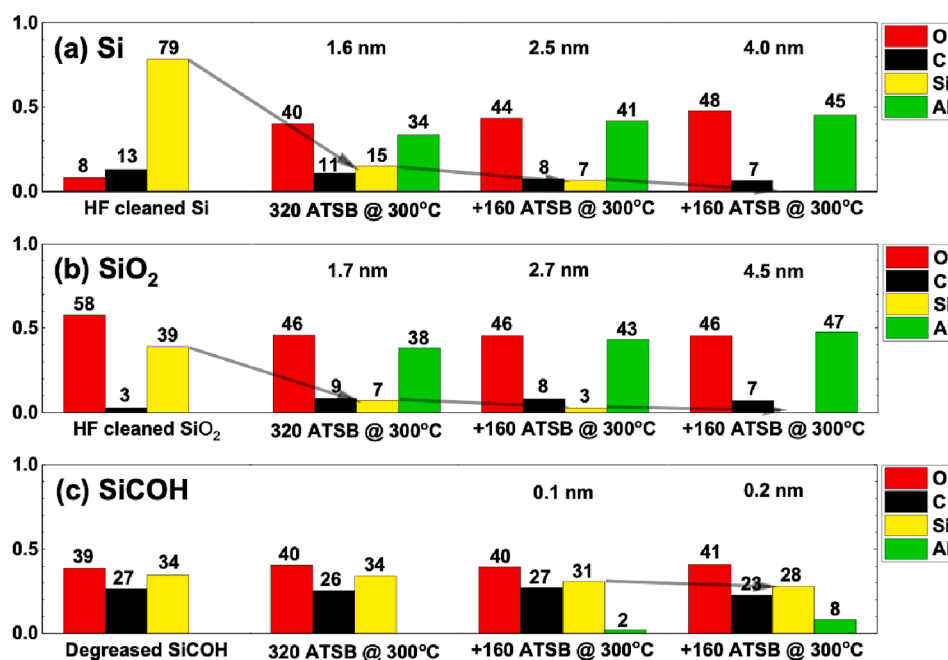


Fig. 1. Analysis of AlO_x Pulsed CVD with ATSB at 300 $^\circ\text{C}$ (10 s purge time). XPS chemical composition of (a) HF cleaned Si, (b) HF cleaned SiO_2 , and (c) degreased SiCOH during AlO_x pulsed CVD with ATSB.

process window for the selective pulsed CVD.

3.2. Selectivity of the AlO_x pulsed CVD with aluminum tri-sec butoxide and TMA

Pulsed CVD with ATSB and TMA was tested to determine if adding TMA increases the selectivity of the AlO_x CVD. In each supercycle, one pulse of TMA was dosed, and the number of sequential ATSB pulses varied from 80 to 160 at 300 °C sample temperature. The 1st test was done with one pulse of TMA and 160 pulses of ATSB per supercycle. (The XPS analysis of the CVD process is shown in Supporting Information Fig. S7.) As shown in Fig. S7, after six supercycles, the AlO_x thickness on Si and SiO_2 were 5.9 and 6.5 nm, respectively, while less than a monolayer (~ 0.2 nm) of AlO_x was deposited on SiCOH . Compared to the selectivity of the AlO_x CVD with ATSB only at 300 °C in Fig. 1, ~ 2 nm of more AlO_x was selectively deposited.

To check if a further increase in selectivity can be achieved, more frequent TMA pulsing was tested with one pulse of TMA and 120 pulses of ATSB per supercycle at 300 °C sample temperature, which is shown in Fig. 2 (X-ray photoelectron spectra of each element-specific binding region are shown in Supporting Information Fig. S8.) The 1st 8 supercycles showed slow growth as the precursor slowly nucleated on Si and SiO_2 surfaces with around 3 nm of AlO_x deposition. After additional 10 supercycles, around 10 and 12 nm of AlO_x were selectively deposited on Si and SiO_2 in preference to SiCOH (~ 0.2 nm). This selectivity was higher than the CVD process with ATSB and the CVD process with less TMA pulse (one pulse of TMA and 160 pulses of ATSB per supercycle).

To check selectivity with even higher TMA frequency supercycles, an additional sample set with one pulse of TMA and 80 ATSB pulses per supercycle was tested at 300 °C sample temperature (The XPS analysis of the CVD process is shown in Supporting Information Fig. S9.) After 32 supercycles, SiCOH remained nuclei-free. However, the growth rate slowed down both on Si and SiO_2 : AlO_x growth rate during each dosing changed as 0.100 nm/cycle \rightarrow 0.050 nm/cycle \rightarrow 0.037 nm/cycle on Si and 0.175 nm/cycle \rightarrow 0.075 nm/cycle \rightarrow 0.050 nm/cycle on SiO_2 . It is hypothesized that TMA reacts on oxide nuclei formed by metal alkoxide precursor (ex: ATSB, $\text{Hf}(\text{O}^i\text{Bu})_4$, and $\text{Ti}(\text{O}^i\text{Pr})_4$) and leaves a less reactive methyl bond on the surface [3]. It is hypothesized that as fewer ATSB

pulses are dosed per cycle with the same number of TMA pulse, fewer reactive AlO_x nuclei are formed during the ATSB half cycle. Therefore, the density of reactive sites after the TMA half-cycle decreased as the number of ATSB pulses per supercycle decreased, inducing growth inhibition. It is also consistent with the growth with one pulse of TMA and 120 pulses of ATSB per supercycle (Fig. 2) being slower than the growth with one pulse of TMA and 160 pulses of ATSB per supercycle (Fig. S7) as shown in Supporting information Fig. S10. Further growth mechanisms for the AlO_x CVD with TMA and ATSB will be discussed below.

The periodical pulsing of TMA helped increase the selective AlO_x deposition, but too frequent TMA pulsing stopped the oxide growth on growth surfaces such as Si and SiO_2 . Therefore, it was found that one pulse of TMA and 120 pulses of ATSB per supercycle was the optimal process condition to achieve the highest selectivity at 300 °C sample temperature. An additional test with 120 pulses of ATSB dosing followed by one pulse of TMA per supercycle tested whether the order of two precursors affects the selectivity. However, as shown in XPS analysis in Supporting Information Fig. S11, similar selectivity (9 nm on Si, 11 nm on SiO_2 vs. 0.2 nm on SiCOH) was achieved, proving the order of precursors does not affect the selectivity.

The CVD process with TMA and ATSB was tested at a higher sample temperature, 330 °C. The TMA + ATSB CVD process (one pulse of TMA and 120 pulses of ATSB per supercycle), optimized at 300 °C sample temperature, was tested at 330 °C. However, as shown in Fig. 3, the amount of selective AlO_x deposition on Si and SiO_2 was similar to that achieved at 300 °C with the same process. (X-ray photoelectron spectra of each element-specific binding region are shown in Supporting Information Fig. S12.) After 5 supercycles, around 10 nm and 11 nm of AlO_x were selectively deposited on Si and SiO_2 , respectively, while less than a monolayer (0.2 nm) was deposited on SiCOH . Similar to the AlO_x CVD with ATSB only, the selectivity of the AlO_x CVD with ATSB and TMA was not affected by the sample temperature. This similarity in both CVD processes is consistent with the nucleation of metal alkoxide precursor on nonreactive SiCOH surfaces determining the limit of selectivity [1].

Even with the similar selectivity in both temperatures, it was observed that ATSB had a higher growth rate on Si and SiO_2 at 330 °C than at 300 °C. Fig. 4 shows the AlO_x film growth from ATSB pulsed CVD at 300 °C and 330 °C. (The growth curve data is from the result in Figs. 1

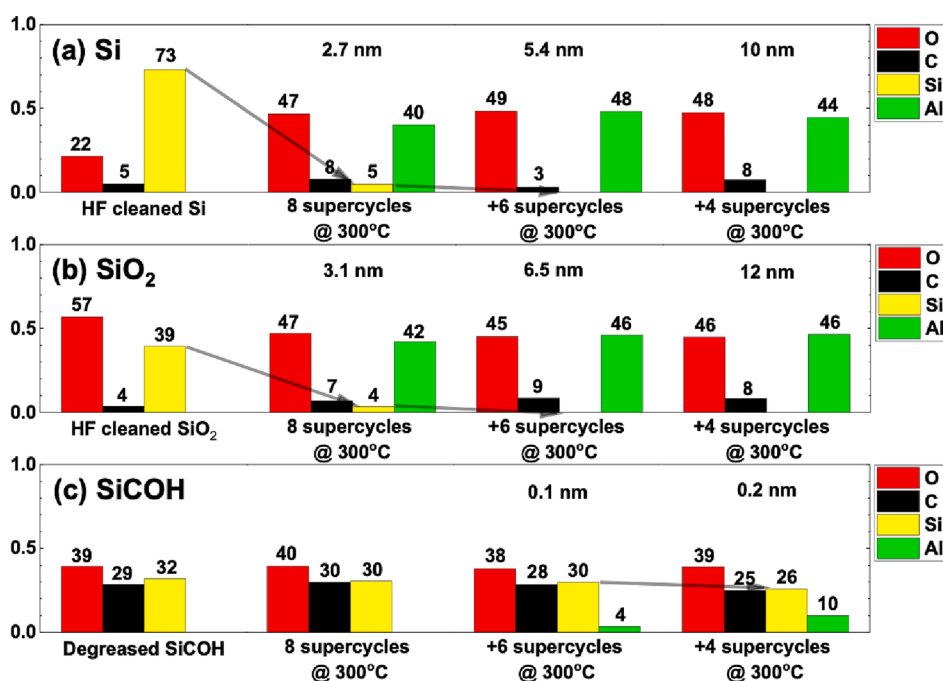


Fig. 2. Analysis of AlO_x Pulsed CVD with one pulse of TMA and 120 pulses of ATSB per supercycle at 300 °C. XPS chemical composition of (a) HF cleaned Si, (b) HF cleaned SiO_2 , and (c) degreased SiCOH during AlO_x pulsed CVD with ATSB and TMA.

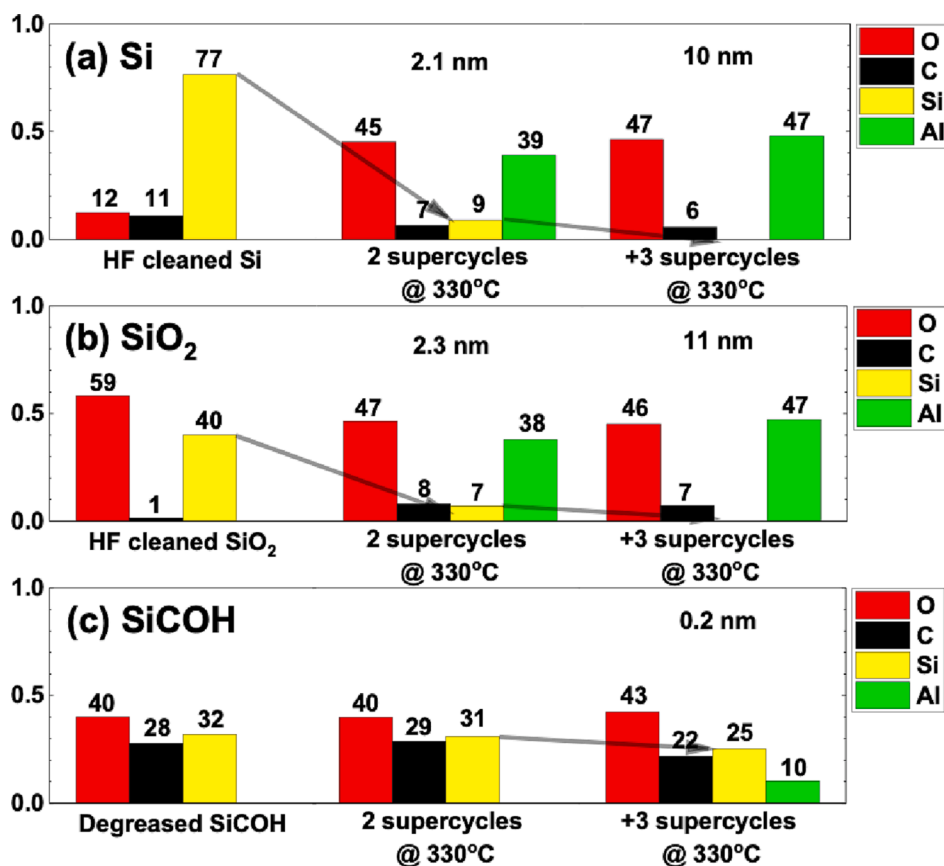


Fig. 3. Analysis of AlO_x Pulsed CVD with one pulse of TMA and 120 pulses of ATSB per supercycle at 330 °C. XPS chemical composition of (a) HF cleaned Si, (b) HF cleaned SiO₂, and (c) degreased SiCOH during AlO_x pulsed CVD with ATSB and TMA.

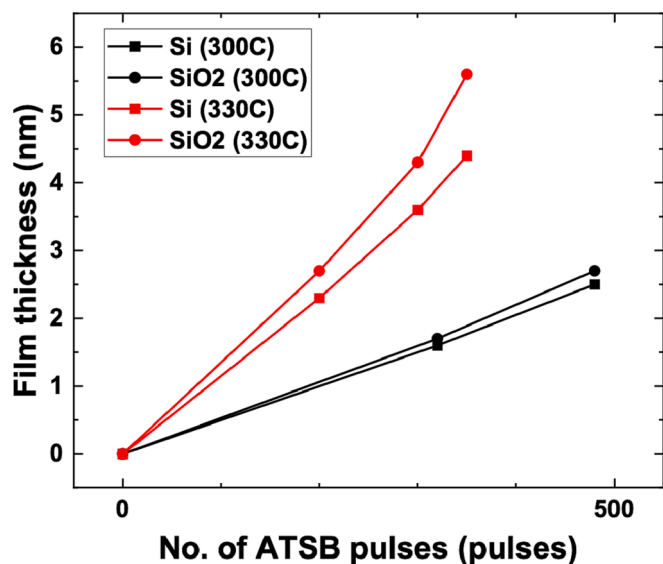


Fig. 4. The growth curve of AlO_x Pulsed CVD with ATSB on Si (square) and SiO₂ (circle) at 300 °C (black) and 330 °C (red). (For interpretation of the references to colour in this figure legend, the reader is referred to the web version of this article.)

and S6.) With a similar number of ATSB pulses, around 2x faster film growth was observed on both Si and SiO₂ at 330 °C. A similar tendency was observed from TMA + ATSB CVD as one pulse of TMA and 120 pulses of ATSB showed faster film growth at 330 °C (Fig. 3) than at 300 °C (Fig. 2) as shown in Supporting information Fig. S13. The data is

consistent with more ATSB thermally decomposes and induces deposition at higher sample temperature. From the TMA + ATSB CVD process study at 300 °C sample temperature, periodical TMA pulses helped increase the selectivity, but excess TMA per a certain amount of ATSB nucleation could inhibit the film growth. Since ATSB had a higher growth rate at 330 °C, it was hypothesized that more frequent TMA could be added in each supercycle at 330 °C, thereby increasing selectivity. The CVD process with more frequent TMA was tested to prove the hypothesis. In each supercycle, the number of ATSB pulses was decreased from 120 to 80 to increase the TMA frequency. This TMA richer process showed growth inhibition at 300 °C sample temperature, as shown in Supporting Information Fig. S9. However, the TMA richer process showed decent film growth without a growth inhibition at 330 °C, as shown in Fig. 5. (X-ray photoelectron spectra of each element-specific binding region are shown in Supporting Information Fig. S14.) After 15 supercycles, 12 nm and 14 nm of AlO_x were deposited on Si, and SiO₂, respectively, with small nucleation (~0.2 nm) on SiCOH. In conclusion, more frequent TMA could be implemented at a higher sample temperature (330 °C) to increase the selectivity. The authors expect that even higher selectivity can be achieved by increasing the sample temperature above 330 °C; unfortunately, 330 °C was the limit of the sample heating system.

3.3. Mechanism and nanoscale selectivity of the AlO_x pulsed CVD (TMA + ATSB)

Based on the above study, the proposed mechanism of the AlO_x pulsed CVD with ATSB and TMA is shown in Fig. 6. ATSB can adsorb (physisorb) on the sample surfaces. Due to high sample temperature, it is hypothesized that a portion of the sec-butoxide ligands thermally decompose and form reactive OH ligands (Al-OH). The rest of sec-

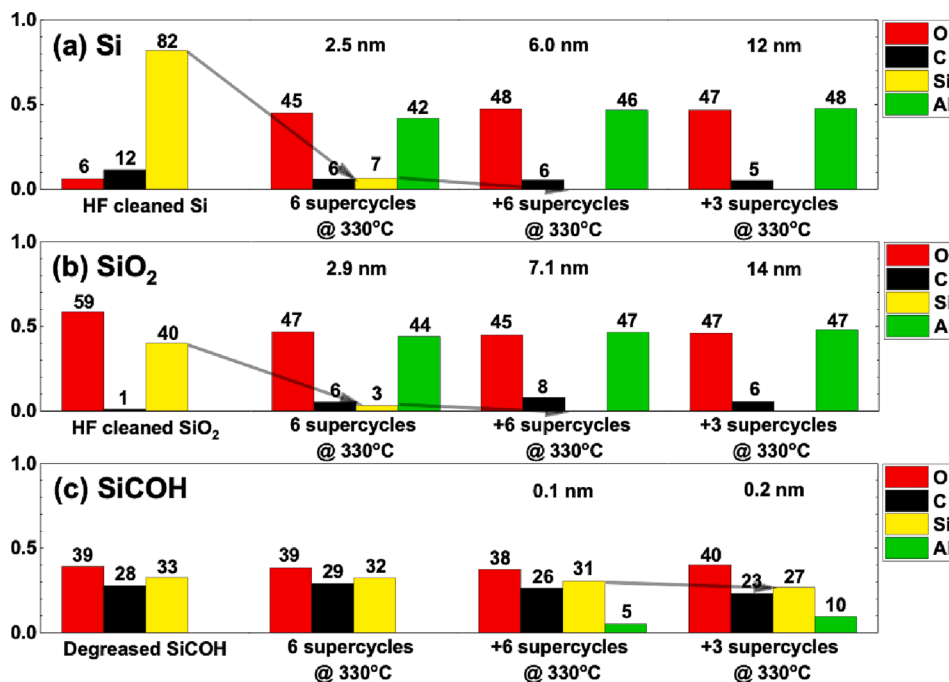


Fig. 5. Analysis of AlO_x Pulsed CVD with one pulse of TMA and 80 pulses of ATSB per supercycle at 330 °C. XPS chemical composition of (a) HF cleaned Si, (b) HF cleaned SiO₂, and (c) degreased SiCOH during AlO_x pulsed CVD with ATSB and TMA.

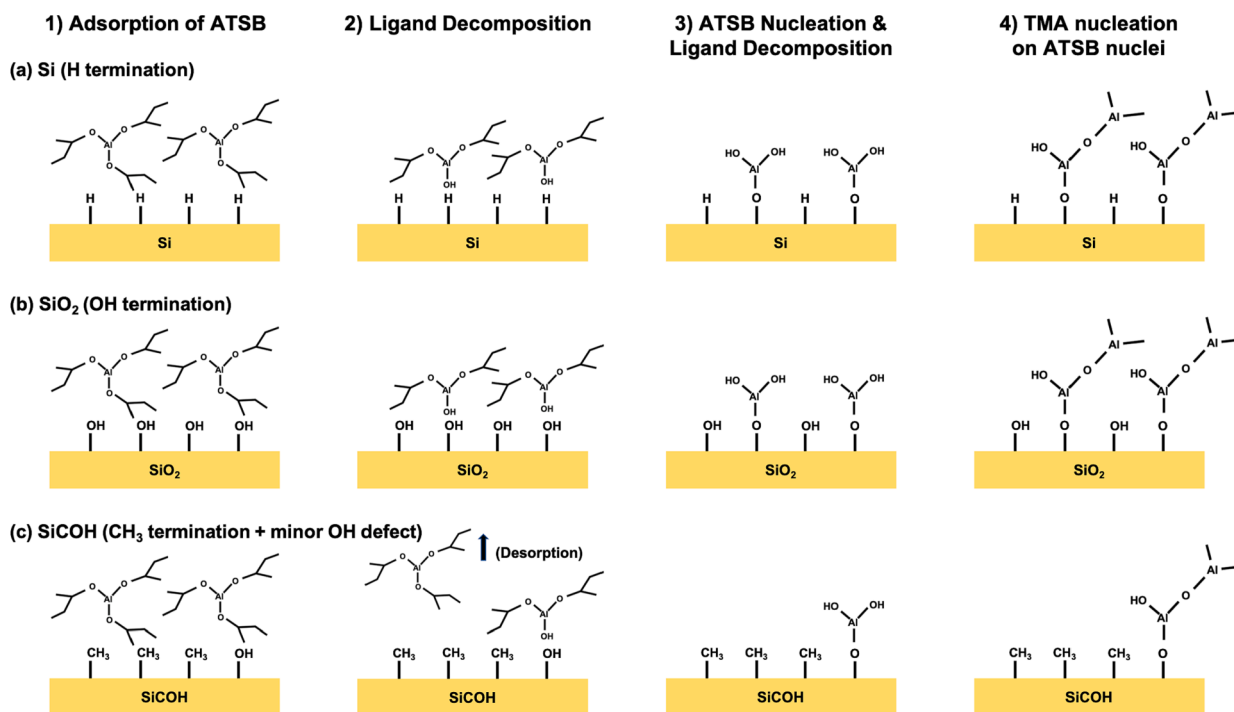


Fig. 6. Proposed reaction mechanism of the AlO_x Pulsed CVD with TMA and ATSB. On (a) Si and (b) SiO₂, ATSB readily adsorbs and undergoes thermal decomposition due to the high density of reactive sites. On (c) SiCOH, there are only minor OH defective nucleation sites; thus, only a few ATSB nucleate while most ATSB desorb away. TMA can react on ATSB nuclei on surfaces, critically suppressing the further nucleation on SiCOH by leaving less reactive methyl ligands.

butoxide ligands desorb. These OH ligands on adsorbed ATSB can react with H or OH bonds on Si and SiO₂, respectively. Si and SiO₂ have a high density of reactive sites, so ATSB can easily nucleate on them. However, the SiCOH surface has less reactive CH₃ bonds with only a minor number of OH defect sites; therefore, only a few adsorbed ATSB can react with the minor OH sites, and most ATSB are desorbed from the SiCOH surface. Conversely, TMA can react with OH bonds on ATSB nuclei.

However, TMA does not have oxygen in its ligands but only has less reactive methyl ligands. Therefore, when TMA reacts with AlO_x nuclei on the surface, it reduces the number of reactive sites and replaces them with less reactive methyl sites. For Si and SiO₂, unless too much TMA is dosed (such as the experiment in Fig. S9), there are still enough H or OH reactive sites for sequential film growth. However, as SiCOH has very few reactive sites or AlO_x nuclei, their reaction with TMA critically

suppresses the further nucleation, inducing higher selective deposition with periodical TMA pulse during ATSB pulses.

Based on the mechanism, the AlO_x CVD with ATSB and TMA can be applied to other surfaces with OH bonds in preference to SiCOH. Metal, such as Cu, tends to form a metal oxide layer on the surface. Therefore, the AlO_x CVD with ATSB and TMA was dosed on Cu/SiCOH nanoscale patterned samples to test the process for nanoscale fabrication. For the AlO_x deposition, one pulse of TMA and 80 pulses of ATSB were dosed per supercycle at 330 °C sample temperature, which showed the highest selectivity.

As shown in XPS chemical composition in Supporting Information Fig. S15, the passivation on the Cu region of the patterned sample desorbed during the UHV anneal (350 °C 10 min) before the deposition process; the carbon fraction decreased, and the Cu fraction increased after the UHV anneal. This proves that the passivation selectively passivated the damaged SiCOH. After 6 supercycles of the AlO_x CVD process using one pulse of TMA and 80 pulses of ATSB per supercycle at 330 °C, the Cu peak was fully attenuated, consistent with selective deposition on the Cu surface. The Si percentage from the SiCOH surface of the patterned sample also decreased from 29 % to 9 %, while the blanket SiCOH was still clean.

Fig. 7 shows the cross-sectional STEM image of the patterned sample after the CVD process in Fig. S15 using one pulse of TMA and 80 pulses of ATSB per supercycle at 330 °C. The patterned sample surface was composed of Cu and SiCOH with around 90 nm and 50 nm widths, respectively. From the STEM images, around 10 nm of AlO_x was selectively deposited on the Cu surface. The selective deposition was confirmed by energy dispersive X-ray (EDX) analysis in Fig. 7B and C. However, AlO_x had an isotropic growth that induced growth over the SiCOH surface (the red circled region in Fig. 7A). Since ~10 nm of AlO_x

film was deposited on the Cu region with isotropic growth, some X-ray signals from the SiCOH surface were blocked, as illustrated in detail in Supporting Information Fig. S16. This is consistent with the Si percentage decreasing on the patterned sample. In addition, the AlO_x film showed a smooth surface in the STEM images. (see confirmation by AFM below). By combining with selective AlO_x etch process [27] as an etch-back process, it could be possible to remove any unwanted nuclei from the SiCOH surface.

3.4. Film morphology and electrical characteristics of the AlO_x film

The ex-situ atomic force microscopy (AFM) was employed to check the film roughness. Fig. 8 shows the AFM images of the AlO_x film on (a) Si and (b) SiO_2 , deposited by the pulsed CVD with one pulse of TMA and 80 pulses of ATSB per supercycle at 330 °C sample temperature. The AlO_x film showed a smooth surface with 0.4–0.5 nm RMS roughness. This is advantageous compared to other oxides such as TiO_2 and HfO_2 , which tend to form a rough surface with nm scale RMS roughness as film thickness increases due to the crystallization. [1,28].

Capacitance-voltage (C-V) and leakage current (I-V) were measured to check the AlO_x film's characteristics as a dielectric material. A capacitor was made on 15 nm AlO_x film on a Si sample with Ni dot top electrode deposited. The C-V and I-V characteristics were measured from -2 V to 2 V, as shown in Fig. 9; however, similar results were obtained by the split I-V and C-V methods. The dielectric constant of the AlO_x film, estimated from the C-V curve (Fig. 9a), was around 4, which is lower than the usual dielectric constant of Al_2O_3 . The lower dielectric constant is consistent with the AlO_x film in this process being oxygen-deficient [29,30]. The XPS chemical composition from Figs. 1, 2, 3, and 5 showed that the selective AlO_x CVD process had around a 1:1 ratio

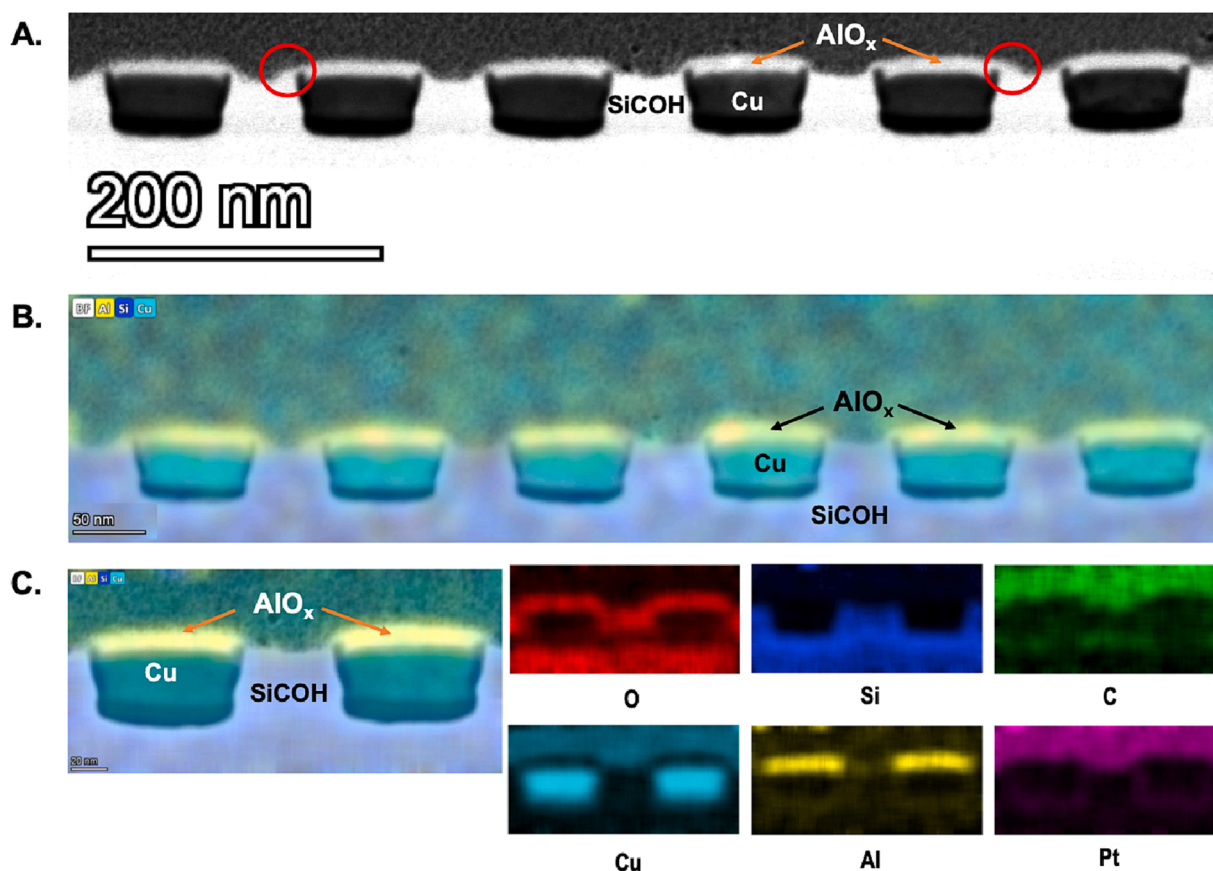


Fig. 7. STEM Analysis of Selective AlO_x Pulsed CVD with ATSB and TMA on a Nanoscale Patterned Sample. One pulse of TMA and 80 pulses of ATSB were dosed per supercycle at 330 °C. (A) Wide view STEM image and (B) EDX image of Cu/SiCOH patterned sample after 6 supercycles of AlO_x pulsed CVD with ATSB and TMA. (B) Magnified view of EDX superposition and single element images.

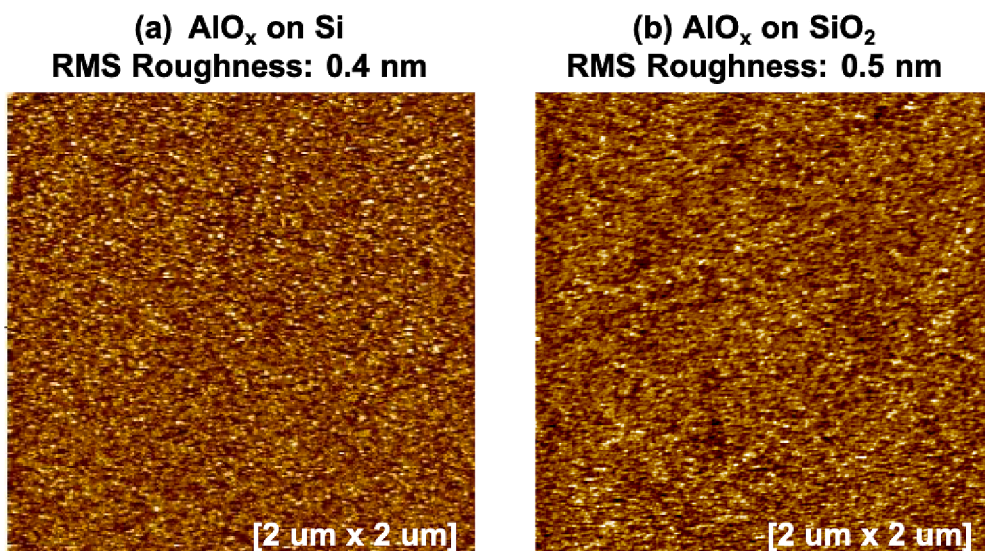


Fig. 8. AFM image of AlO_x films on Si and SiO_2 deposited by the Pulsed CVD with ATSB and TMA at 330°C . AFM image of (a) AlO_x film on Si and (b) AlO_x film on SiO_2 deposited by the pulsed CVD with one pulse of TMA and 80 pulses of ATSB per supercycle at 330°C sample temperature.

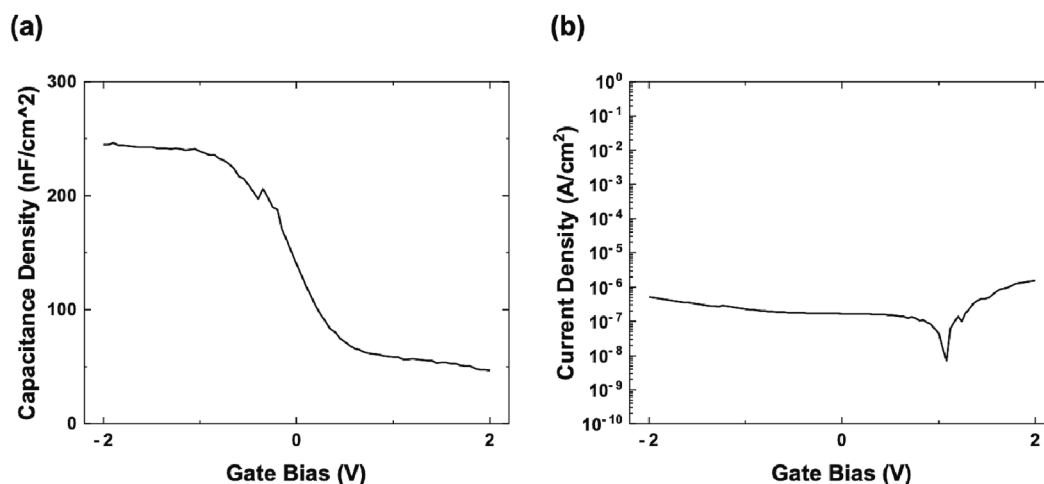


Fig. 9. Electrical characteristics of the AlO_x film deposited by the Pulsed CVD with ATSB and TMA at 330°C . (a) Capacitance per unit area (1 MHz) and (b) Leakage current density of the AlO_x film on Si substrate. The AlO_x film thickness was around 15 nm.

for Al_2O_3 , which means the AlO_x film was close to Al_2O_3 rather than Al_2O_3 . The 1:1 Al:O ratio continued even after the post-deposition anneal, as shown in Supporting Information Fig. S17. Fig. S17 showed that the bulk of AlO_x film also had a 1:1 Al:O ratio. The oxygen deficiency of the film could be because the process was water-free [31]. The leakage current after the post-deposition anneal was low (around 10^{-6} A/cm^2 at ± 2 V as shown in Fig. 9b), showing the insulating behavior of the AlO_x film. In conclusion, as the selectively deposited AlO_x film was non-stoichiometric, it did not show the same behavior as Al_2O_3 ; however, it showed low k dielectric behavior with a dielectric constant close to SiO_2 .

4. Conclusion

Inherent selective deposition of AlO_x through thermal pulsed CVD was studied. Aluminum tri-sec butoxide (ATSB) is a liquid metal alkoxide precursor, which has oxygen in each ligand. Through thermal decomposition, it can form an oxide film without a secondary oxygen precursor, such as water; it enables halogen-free and water-free selective oxide deposition, which can protect water-sensitive insulators (ex: SiCOH) and halogen-sensitive metal (ex: Cu) substrates. Due to the

reactivity difference of ATSB on Si, SiO_2 , and SiCOH , around 4–5 nm of AlO_x film was selectively deposited on Si and SiO_2 before significant nuclei were deposited on SiCOH . With the combination of oxygen-rich metal alkoxide precursor ATSB and strong oxygen scavenger TMA, selective AlO_x pulsed CVD was developed. An adequate amount of TMA per supercycle inhibited the nucleation on SiCOH and increased the selective deposition on Si and SiO_2 to 12–14 nm at 330°C sample temperature. The film was smooth with 0.4–0.5 nm RMS roughness. As the film was non-stoichiometric with a 1:1 Al:O ratio, the dielectric constant of the AlO_x was around 4, which is lower than the usual Al_2O_3 dielectric constant. The film showed around 10^{-6} A/cm^2 of leakage current, proving the film has insulating behavior. The AlO_x pulsed CVD with ATSB and TMA showed around 10 nm of selective deposition on the Cu region of the Cu/ SiCOH nanoscale patterned sample. The AlO_x pulsed CVD combines the attributes of selectivity over 10 nm, a smooth film formation, and the potential to be readily etched since it is a uniform amorphous oxide. Therefore, it will be suitable as a spacer or mask in nanoscale MOSFET fabrication.

Associated Content.

Supporting Information.

The following files are available free of charge.

A schematic of the vacuum chamber for AlO_x CVD and XPS analysis, XPS Spectra Analysis for AlO_x Pulsed CVD with ATSB at 300 °C (10 s purge time), XPS Analysis of AlO_x Pulsed CVD with ATSB at 300 °C (60 s purge time), XPS Analysis of AlO_x Pulsed CVD with ATSB at 300 °C (240 s purge time), The growth curve of AlO_x Pulsed CVD with ATSB on Si and SiO₂ at 300 °C with different purge times, XPS Analysis of AlO_x Pulsed CVD with ATSB at 330 °C (10 s purge time), XPS Analysis of AlO_x Pulsed CVD with one pulse of TMA and 160 pulses of ATSB per supercycle at 300 °C, XPS Spectra Analysis for AlO_x Pulsed CVD with one pulse of TMA and 120 pulses of ATSB per supercycle at 300 °C, XPS Analysis of AlO_x Pulsed CVD with one pulse of TMA and 80 pulses of ATSB per supercycle at 300 °C, The growth curve of AlO_x Pulsed CVD with ATSB and TMA on Si and SiO₂ with different TMA relative frequency, XPS Analysis of AlO_x Pulsed CVD with 120 pulses of ATSB and one pulse of TMA per supercycle (reverse order of precursors) at 300 °C, XPS Spectra Analysis for AlO_x Pulsed CVD with one pulse of TMA and 120 pulses of ATSB per supercycle at 330 °C, The growth curve of AlO_x Pulsed CVD with 1 pulse of TMA and 120 pulse of ATSB per supercycle on Si and SiO₂ at 300 °C and 330 °C, XPS Spectra Analysis for AlO_x Pulsed CVD with one pulse of TMA and 80 pulses of ATSB per supercycle at 330 °C, XPS of Selective AlO_x pulsed CVD with ATSB and TMA on a Cu/ SiCOH Nanoscale Patterned Sample, Illustration for the decrease in Si % on the Cu/SiCOH patterned sample after the deposition, XPS chemical composition of the AlO_x film, deposited by the selective CVD with ATSB and TMA at 330 °C, before and after each post-deposition anneal. (PDF).

CRedit authorship contribution statement

Yunil Cho: Conceptualization, Methodology, Formal analysis, Investigation, Writing – original draft. **James Huang:** Methodology, Formal analysis, Investigation. **Zichen Zhang:** Formal analysis. **Kesong Wang:** Formal analysis. **Ping-che Lee:** Formal analysis. **Chanyoung Kim:** Investigation. **Keith Wong:** Writing – review & editing, Resources. **Srinivas Nemani:** . **Ellie Yieh:** Supervision. **Andrew C. Kummel:** Writing – review & editing, Supervision.

Declaration of Competing Interest

The authors declare that they have no known competing financial interests or personal relationships that could have appeared to influence the work reported in this paper.

Data availability

No data was used for the research described in the article.

Acknowledgements

Funding support from Applied Materials is gratefully acknowledged. The electrical measurements were facilitated by the San Diego Nanotechnology Infrastructure (SDNI) which is supported by the National Science Foundation (NSF) to Nano3 (Grant ECCS-1542148).

Appendix A. Supplementary material

Supplementary data to this article can be found online at <https://doi.org/10.1016/j.apsusc.2023.156824>.

References

- [1] Y. Cho, C.F. Ahles, J.Y. Choi, J. Huang, A. Jan, K. Wong, S. Nemani, E. Yieh, A. C. Kummel, Inherently selective water-free deposition of titanium dioxide on the nanoscale: implications for nanoscale patterning, *ACS Appl. Nano Mater.* 5 (1) (2022) 476–485.
- [2] A.J.M. Mackus, A.A. Bol, W.M.M. Kessels, The use of atomic layer deposition in advanced nanopatterning, *Nanoscale* 6 (2014) 10941–10960.
- [3] J. Huang, Y. Cho, Z. Zhang, A. Jan, K.T. Wong, S. Nemani, E. Yieh, A.C. Kummel, Selective pulsed chemical vapor deposition of water-free TiO₂/Al₂O₃ and HfO₂/Al₂O₃ nanolaminates on Si and SiO₂ in preference to SiCOH, *ACS Appl. Mater. Interfaces* 14 (13) (2022) 15716–15727.
- [4] Y. Cho, J. Huang, C.F. Ahles, Z. Zhang, K. Wong, S. Nemani, E. Yieh, A.C. Kummel, Inherent selective pulsed chemical vapor deposition of amorphous hafnium oxide/titanium oxide nanolaminates, *Appl. Surf. Sci.* 600 (2022), 154010.
- [5] H.P. Chen, Y.H. Wu, H.Y. Huang, C.H. Tsai, S.K. Lee, C.C. Lee, T.H. Wei, H.C. Yao, Y.C. Wang, C.Y. Liao, H.K. Chang, C.W. Lu, W.S. Shue, C. Min, Fully self-aligned via integration for interconnect scaling beyond 3nm node, *IEEE IEDM* 21–486 (2021).
- [6] S.V. Nguyen, H. Shobha, C.B. Peethala, T. Haigh, H. Huang, J. Li, J. Demarest, B. Haran, D. Hausmann, P. Lemaire, K. Sharma, P. Ramani, A. Mahorowala, Selective deposition of AlO_x for Fully Aligned Via in nano Cu interconnects, *IEEE IITC* (2021) S7–S14.
- [7] M. Yang, A.A.I. Aarnink, J. Schmitz, A.Y. Kovalgin, Inherently area-selective hot-wire assisted atomic layer deposition of tungsten films, *Thin Solid Films* 649 (2018) 17–23.
- [8] J.Y. Choi, C.F. Ahles, Y. Cho, A. Anurag, K.T. Wong, S.D. Nemani, E. Yieh, A. C. Kummel, Selective pulsed chemical vapor deposition of water-free HfO_x on Si in preference to SiCOH and passivated SiO₂, *Appl. Surf. Sci.* 512 (2020), 145733.
- [9] J.Y. Choi, C.F. Ahles, R. Hung, N. Kim, A.C. Kummel, Selective atomic layer deposition of MoSi_x on Si (001) in preference to silicon nitride and silicon oxide, *Appl. Surf. Sci.* 462 (2018) 1008–1016.
- [10] P.C. Lemaire, M. King, G.N. Parsons, Understanding inherent substrate selectivity during atomic layer deposition: effect of surface preparation, hydroxyl density, and metal oxide composition on nucleation mechanisms during tungsten ALD, *J. Chem. Phys.* 146 (2017), 052811.
- [11] T. Suh, Y. Yang, P. Zhao, K.U. Lao, H.Y. Ko, J. Wong, R.A. DiStasio Jr, J. R. Engstrom, Competitive adsorption as a route to area-selective deposition, *ACS Appl. Mater. Interfaces* 12 (2020) 9989–9999.
- [12] D. Bobb-Semple, K.L. Nardi, N. Draeger, D.M. Hausmann, S.F. Bent, Area-selective atomic layer deposition assisted by self-assembled monolayers: a comparison of Cu Co, W, and Ru, *Chem. Mater.* 31 (2019) 1635–1645.
- [13] F.S.M. Hashemi, S.F. Bent, Sequential regeneration of self-assembled monolayers for highly selective atomic layer deposition, *Adv. Mater. Interfaces* 3 (2016) 1600464.
- [14] F.S.M. Hashemi, C. Prasittichai, S.F. Bent, A new resist for area selective atomic and molecular layer deposition on metal-dielectric patterns, *J. Phys. Chem. C* 118 (2014) 10957.
- [15] F.S.M. Hashemi, B.R. Birchansky, S.F. Bent, Selective deposition of dielectrics: limits and advantages of alkanethiol blocking agents on metal–dielectric patterns, *ACS Appl. Mater. Interfaces* 8 (2016) 33264–33272.
- [16] A. Mameli, B. Karasulu, M.A. Verheij, B. Barcones, B. Macco, A.J.M. Mackus, W. M.M.E. Kessels, F. Roozeboom, Area-selective atomic layer deposition of ZnO by area activation using electron beam-induced deposition, *Chem. Mater.* 31 (2019) 1250–1257.
- [17] A. Mameli, Y. Kuang, M. Aghaee, C.K. Ande, B. Karasulu, M. Creatore, A.J. M. Mackus, W.M.M. Kessels, F. Roozeboom, Area-selective atomic layer deposition of In₂O₃: H using a u-plasma printer for local area activation, *Chem. Mater.* 29 (2017) 921–925.
- [18] A.J.M. Mackus, J.J.L. Mulders, M.C.M. van de Sanden, W.M.M. Kessels, Local deposition of high-purity Pt nanostructures by combining electron beam induced deposition and atomic layer deposition, *J. Appl. Phys.* 107 (2010), 116102.
- [19] S. Atanasov, B. Kalanyan, G.N. Parsons, Inherent substrate-dependent growth initiation and selective-area atomic layer deposition of TiO₂ using “water-free” metal-halide/metal alkoxide reactants, *J. Vac. Sci. Technol. A* 34 (2016) 01A148.
- [20] V. McGahay, Porous dielectrics in microelectronic wiring applications, *Materials* 3 (2010) 536–562.
- [21] A. Grill, Plasma enhanced chemical vapor deposited SiCOH dielectrics: from low-k to extreme low-k interconnect materials, *J. Appl. Phys.* 93 (2003) 1785.
- [22] D.C. Edelstein, S.M. Gates, A. Grill, M. Lane, R.D. Miller, D.A. Neunmayer, S.V. Nguyen, SiCOH dielectric material with improved toughness and improved Si-C bonding, semiconductor device containing the same, and method to make the same, US 2005/0194619 A1.
- [23] D.F. Canaperi, S.V. Nguyen, D. Priyadarshini, H.K. Shobha, Advanced ultra low k SiCOH dielectrics prepared by built-in engineered pore size and bonding structured with cyclic organosilicon. US 9209017 B2.
- [24] L. Cao, F. Mattelaer, T. Sajavaara, J. Dendooven, C. Detavernier, A liquid alkoxide precursor for the atomic layer deposition of aluminum oxide films, *J. Vac. Sci. Technol. A* 38 (2) Mar/Apr (2020).
- [25] T.L. Liu, S.F. Bent, Area-selective atomic layer deposition on chemically similar materials: achieving selectivity on oxide/oxide patterns, *Chem. Mater.* 33 (2) (2021) 513–523.
- [26] T. Oszinda, M. Schaller, S.E. Schulz, Chemical repair of plasma damaged porous ultra low-k SiOCH film using a vapor phase process, *J. Electrochem. Soc.* 157 (2010) H1140.
- [27] X. Yang, J.C. Woo, D.S. Um, C.I. Kim, Dry etching of Al₂O₃ thin films in O₂/BCl₃/Ar inductively coupled plasma, *Trans. Electr. Electron. Mater.* 11 (5) (2010) 202.
- [28] R. Rammula, J. Aarik, H. Mandar, P. Ritslaid, V. Sammelselg, Atomic layer deposition of HfO₂: Effect of structure development on growth rate, morphology and optical properties of thin films, *Appl. Surf. Sci.* 257 (2010) 1043–1052.

- [29] F. Hamelmann, U. Heinzmann, A. Szekeres, N. Kirov, T. Nikolova, Deposition of silicon oxide thin films in TEOS with addition of oxygen to the plasma ambient: IR spectra analysis, *J. Optoelectron. Adv. Mater.* 7 (1) (2005) 389–392.
- [30] M. Kassmi, J. Pointet, P. Gonon, A. Bsiesy, C. Vallee, F. Jomni, Low-frequency dielectric properties of intrinsic and Al-doped rutile TiO₂ thin films grown by the atomic layer deposition technique, *J. Appl. Phys.* 119 (2016), 244101.
- [31] A.E. Kasmi, Z.Y. Tian, H. Vieker, A. Beyer, T. Chafik, Innovative CVD synthesis of Cu₂O catalysts for CO oxidation, *Appl. Catal. B* 186 (2016) 10–18.